Determination of Schottky barrier profile at Pt/$SrTiO_3$:Nb junction by x-ray photoemission

Naoki Ohashi,[a] Hideki Yoshikawa,[b] Yoshiyuki Yamashita,[b] Shigenori Ueda,[b] Jianyong Li, Hideyo Okushi, Keisuke Kobayashi,[c] and Hajime Haneda
National Institute for Materials Science (NIMS), 1-1 Namiki, Tsukuba 305-0044, Japan

(Received 8 September 2012; accepted 3 December 2012; published online 20 December 2012; publisher error corrected 29 January 2013)

The platinum/[niobium-doped strontium titanate] junction (Pt/$SrTiO_3$:Nb) was investigated by x-ray photoemission (XPE) spectroscopy. Aluminum Kα and synchrotron radiation (6 keV) were used to obtain XPE spectra with different probing depths. The broadening and shift of the XPE peaks for $SrTiO_3$:Nb, which resulted from the formation of a potential barrier at the interface, were quantitatively analyzed by fitting simulations. The barrier height was calculated to be 0.7–0.8 regardless of the Nb concentration. Furthermore, the XPE profile of the junction was reproduced when the permittivity of $SrTiO_3$ was assumed to depend on the electric field. © *2012 American Institute of Physics*. [http://dx.doi.org/10.1063/1.4772628]

Junction structures consisting of perovskite-type oxides, such as strontium titanate ($SrTiO_3$), exhibit a number of interesting and useful functions including the varistor properties of doped $SrTiO_3$ ceramics,[1] thermistor properties of doped barium titatnate,[2] and rectification behavior at metal/$SrTiO_3$ structures.[3] In particular, some junctions made from Nb-doped $SrTiO_3$ ($SrTiO_3$:Nb) show resistance switching (RS) behavior[4,5]—a reversible change of junction resistance between the high and low states by applying a bias of different polarity. RS behavior, which has been observed in many metal oxide-based junctions, is considered to be appropriate for high-speed nonvolatile memory devices.[6,7] Although several models have been proposed to explain RS behavior at metal/$SrTiO_3$:Nb junctions,[4,5,8,9] details of the mechanism are unresolved, hindering further development of these junctions.

The main reason why the RS mechanism has not been understood in detail is that the properties at the metal/$SrTiO_3$:Nb junction cannot be explained by entering the physical parameters of bulk $SrTiO_3$ into an ordinary model of metal/semiconductor Schottky junctions. At ordinary metal/semiconductor junctions, the relative dielectric permittivity (ε_r) of the semiconductor is a constant that is identical to that of bulk.[10] However, for metal/$SrTiO_3$:Nb junctions, the dependence of ε_r on the electric field (E) and temperature (T), as expressed in Eq. (1),[11] is non-negligible[12]

$$\varepsilon_r(E,T) = b(T)/\sqrt{a(T)+E^2}. \quad (1)$$

Here, $a(T)$ and $b(T)$ are temperature-dependent constants and are reported to be $a(T) = [b(T)/\varepsilon(T,\ E=0)]^2$ and $b(T) = 1.37\times10^9 + 4.29\times10^7\,T$ (V/m). Under the condition $E = 0$, ε_r can be approximated by Eq. (2)[13,14]

$$\varepsilon_r(T, E=0) = \frac{1635}{\coth(44.1/T) - 0.937}. \quad (2)$$

In fact, the observed capacitance-voltage (C–V) characteristics at Pt/$SrTiO_3$:Nb junctions deviate from those predicted by ordinary semiconductor junction models assuming a constant ε_r.[12] That measuring the C–V characteristics is an appropriate way to know the potential and donor concentration distributions at junctions is well known. However, the C–V curve becomes less sensitive to donor concentration (N_D) at Pt/$SrTiO_3$:Nb junctions owing to the field dependence of ε_r. This implies that N_D, or potential distribution at the junction cannot be uniquely determined solely from the C–V plot unless we know $\varepsilon(E, T)$ accurately.

This situation motivated us to consider X–ray photoemission (XPE) spectroscopy as a way to determine the potential distribution at metal/$SrTiO_3$ junctions. Indeed, a number of prior studies have reported observing band-bending behavior in $SrTiO_3$ beneath a metal electrode.[15–17] However, the impact of XPE is limited by the short probing depth, which is defined by the inelastic mean free path (IMFP) of photoelectrons. In most cases, the depression layer width at the Schottky junction is at least one order of magnitude larger than the probing depth of soft-x-ray XPE (SXPE). This means that probing the entire depletion layer by SXPE is difficult; moreover, the metal electrode must be very thin to enable XPE measurements for $SrTiO_3$ located beneath a metal electrode. Therefore, in this study, hard-x-ray photoemission (HXPE) spectroscopy was employed to determine the potential curve in $SrTiO_3$:Nb located beneath a metal electrode.

We used commercially available $SrTiO_3$:Nb single crystals with three different Nb-doping levels to prepare Pt/$SrTiO_3$:Nb junctions. Hall measurements revealed that the free electron concentrations (n) at room temperature were 2×10^{20}, 2×10^{19}, and $4\times10^{18}\,cm^{-3}$ for 0.5, 0.05, and 0.01 wt. % Nb-doped $SrTiO_3$, respectively. These n values and Nb concentrations were in good agreement, indicating that free electrons were injected by the Nb donor.

Platinum (Pt) electrodes were deposited on the polished surface of $SrTiO_3$:Nb by the dc sputtering technique, and an ohmic aluminum (Al) electrode was formed on the back side of the crystal by conventional vacuum evaporation. Prior to these deposition processes, some of the $SrTiO_3$:Nb crystals

[a]Author to whom correspondence should be addressed. Electronic mail: OHASHI.Naoki@nims.go.jp.
[b]Present address: Synchrotron X-ray Station at SPring-8, NIMS, 1-1-1 Kouto, Sayo, Hyogo 679-5148, Japan.
[c]Present address: Condensed Matter Science Division, Japan Atomic Energy Agency, Kouto 1-1-1, Sayo-cho, Sayo-gun, Hyogo 679-5148, Japan.

were annealed at 1400 °C in air to improve crystallinity at the surface. The thickness of the Pt electrode was varied (approximately 2–8 mm) by changing the deposition time.

The current-voltage (I–V) relationships of the obtained Pt/$SrTiO_3$:Nb junctions are shown in Fig. 1. All junctions showed rectification behavior, and the magnitude of leakage current increased with the Nb concentration in $SrTiO_3$:Nb. These behaviors are commonly observed at Pt/$SrTiO_3$:Nb junctions.[4,5] Only the junction made from 0.5 wt. % Nb-doped crystal showed hysteresis in the I–V curve. Here, we proceeded to conduct XPE measurements to determine the potential distribution at the junction.

A Σ-Probe spectrometer from Thermo Fisher Scientific K.K. (Yokohama, Japan) equipped with a monochromated Al–$K\alpha$ radiation source was used for the SXPE measurements. Meanwhile, HXPE measurements were performed using a 6-keV incident x-ray beam at the undulator beamline BL15XU of SPring-8, Japan. Details of the instrumental setup at BL15XU are provided elsewhere.[18–21] The origin of the electron binding energy (E_B) was set to the Fermi level (E_F), which was calibrated by measuring the E_F of pure gold.

Figure 2(a) compares the SXPE spectrum of the naked $SrTiO_3$:Nb surface with that of the Pt electrode. The valence band maximum (VBM) of naked $SrTiO_3$:Nb was found at about 3 eV below E_F, indicating that E_F in $SrTiO_3$:Nb was very close to its conduction band minimum (CBM). This result is reasonable because the $SrTiO_3$:Nb crystals were degenerate semiconductors showing nearly constant electron concentrations as a function of temperature. In the HXPE spectra, the VBM of naked $SrTiO_3$:Nb was also found at 3 eV below E_F.

The Ti $2p_{3/2}$ core-level spectra are shown in Fig. 2(b) for SXPE and Fig. 2(c) for HXPE. These spectra were obtained from a sample with a relatively thin Pt electrode (approximately 3 nm). For the sample with a thicker electrode (approximately 7 nm), the XPE originating from $SrTiO_3$:Nb beneath the Pt electrode was not observed by SXPE. In both SXPE and HXPE spectra, the positions of the Ti $2p_{3/2}$ peaks of the naked $SrTiO_3$:Nb surface were identical and the spectral shape for the naked surface was symmetric along the energy axis. Therefore, we do not need to consider surface potential formation at the naked surface because the VBM of $SrTiO_3$ was found at 3 eV below E_F and the spectral shape was symmetric. In Fig. 2, the width of the Ti $2p_{3/2}$ peak for the naked surface was wider in SXPE than in HXPE. This was mostly because the instrumental resolution of the SXPE spectrometer was lower than that of the HXPE spectrometer (≈0.23 eV).

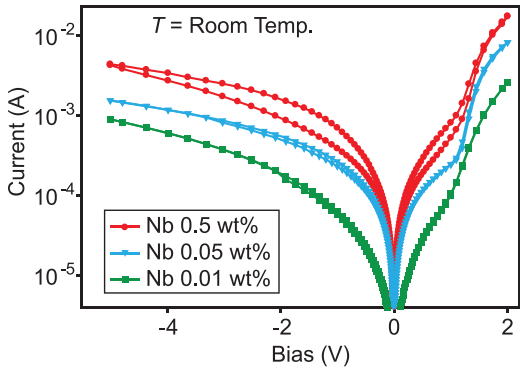

FIG. 1. I-V curve at Pt/$SrTiO_3$:Nb junction with different Nb concentrations.

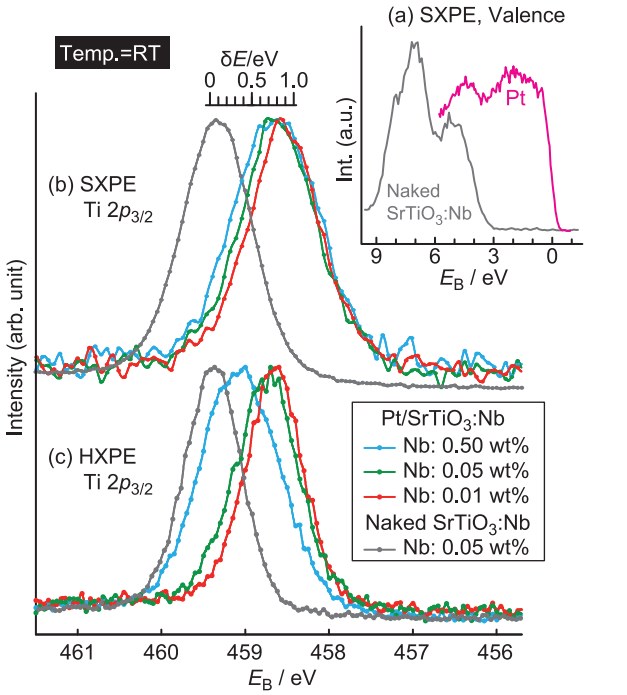

FIG. 2. XPE spectra in valence band and Ti $2p_{3/2}$ range of naked $SrTiO_3$:Nb surface and Pt/$SrTiO_3$:Nb structures. SXPE and HXPE denote XPE excited by soft x-ray (AlKα) and hard x-ray (6 keV), respectively. Numbers in wt. % show Nb-doping concentrations in $SrTiO_3$:Nb crystal.

In contrast to the naked surface, the profile of the Ti $2p_{3/2}$ peak of the Pt/$SrTiO_3$:Nb structures changed with the Nb concentration in the $SrTiO_3$ substrate and the incident X-ray energy. The width of the Ti $2p_{3/2}$ peak of Pt/$SrTiO_3$:Nb structures increased as the Nb concentration increased; this broadening was more obvious in the HXPE spectra. The differences between the SXPE and HXPE spectra were significant for the Pt/$SrTiO_3$:Nb structures made from 0.5 wt. % Nb-doped $SrTiO_3$. In fact, the peak for the 0.5 wt. % Nb-doped sample was close to that for the other two samples in SXPE, whereas it showed a significant shift in HXPE.

The variation of peak shape and shift of peak position observed in the Ti $2p_{3/2}$ core level are usually explained by assuming a potential barrier formed at the Pt/$SrTiO_3$:Nb interface.[15–17] However, there is another possible explanation for the variation in the spectral profile of Ti $2p$ core-level peaks. A mixed-valence state of Ti, such as the coexistence of Ti^{3+} and Ti^{4+}, may account for the shift and broadening of the Ti $2p$ core-level peaks. However, the assumption of a mixed-valence state of Ti is unreasonable because the other core-level peaks in the HXPE spectra, e.g., Sr $3d$ and O $1s$ (not shown), showed a shift and broadening similar to those of the Ti $2p$ core-level peak. Moreover, we cannot explain the difference between the SXPE and HXPE profiles if we assume that the shift and broadening were due to a chemical shift. Therefore, we can safely attribute the shift and broadening of the Ti $2p$ core-level peak to the formation of a potential barrier at the Pt/$SrTiO_3$:Nb interface.

We also note that the magnitude of broadening or shift of the peaks slightly varied from sample to sample for the interface prepared using $SrTiO_3$:Nb crystal with 0.5 wt. % Nb. The range of variation in the peak position was 0.1 eV. This variation will be discussed later.

For quantitative analyses of the shift and broadening of the peak, we performed numerical simulations of the XPE spectra with the model illustrated in Fig. 3. Here, we assume that $SrTiO_3$:Nb is composed of thin slices parallel to the surface and that the observed XPE peaks are produced by integrating the elemental peaks that come from each slice with a different potential energy.

First, we assume that the probability of photoelectrons reaching the electron analyzer is expressed by a simple exponential decay function. A photoelectron, emitted at a certain depth x from the interface (Fig. 3) and moving away from the sample with a take-off angle of θ, can reach the electron analyzer with probability (p), as expressed by Eq. (3)

$$p(x, E_k, \theta) = p_0 \cdot \exp\left[-\frac{x/\cos(90-\theta)}{\delta(E_k)}\right]. \quad (3)$$

Here, p_0 is a pre-exponential parameter for normalization and $\delta(E_k)$ denotes the IMFP of a photoelectron with a kinetic energy of E_k. In this expression, the effects of multiple elastic photoelectron scatterings and the forward scattering that causes the specific dependence of XPE intensity on θ (Ref. 22) are neglected. In the simulations, the IMFP at E_k, (i.e., for Ti 2p, 7.8 nm for HXPE and 2.2 nm for SXPE) was estimated according to the values reported in the literature.[23]

Subsequently, we introduce a Gaussian-based function, Γ, to reproduce the shape of elemental peaks emitted at depth x. When the potential at a certain x is parameterized as $E_c(x)$, the simulated intensity at a certain E_k for an elemental peak centered at $E_c(x)$ is expressed as $\Gamma[E_k, E_c(x)]$ using a Gaussian-based peak form function. Reproduction of instrumental peak broadening is the main purpose of $\Gamma[E_k, E_c(x)]$, which was determined from the Ti $2p_{3/2}$ peak of the naked $SrTiO_3$:Nb surface. With $p(x, E_k, \theta)$ and $\Gamma[E_k, E_c(x)]$, the observed XPE spectrum of $SrTiO_3$:Nb beneath the Pt electrode can be expressed by Eq. (4)

$$I(E_k, \theta) = \int_0^\infty p(x, E_k, \theta) \cdot \Gamma[E_k, E_c(x)]dx. \quad (4)$$

Here, $E_c(x)$ must be described to simulate the XPE profiles. Namely, our purpose is to determine $E_c(x)$ by fitting the observed XPE spectra to the model spectra in order to obtain the potential distribution at Pt/$SrTiO_3$:Nb Schottky junctions. Here, we use Eq. (5) to describe the potential distribution at the junction under the equilibrium state (no external bias).

$$E_c(x) = E_{c\infty} + \frac{\sqrt{ab}\varepsilon_0}{N_D}\left\{\cosh\left[\frac{qN_D}{\sqrt{ab}\varepsilon_0}(W_d - x)\right] - 1\right\} (x \le W_d), \quad (5a)$$

$$= E_{c\infty} \ (x \ge W_d), \quad (5b)$$

where

$$W_d = \frac{b\varepsilon_0}{qN_D}\cosh^{-1}\left[1 + \frac{qN_D}{\sqrt{ab}\varepsilon_0}\phi_{b0}\right]. \quad (5c)$$

This equation describes the potential distribution under the assumption that ε_r of $SrTiO_3$:Nb shows electric field dependence with the temperature-dependent parameters a and b in Eq. (1).[9,11,12] Note that N_D, ϕ_{b0}, and $E_{c\infty}$ denote the donor concentration in $SrTiO_3$, barrier height at the Pt/$SrTiO_3$:Nb junction, and E_k under the flat band condition, respectively.

Figure 4 shows typical results of simulation to examine variation of XPE profile with IMFP employing $\Gamma[E_k, E_c(x)]$ obtained from observed HXPE profile of naked $SrTiO_3$. Here, a potential profile ($E_c(x)$) shown in Fig. 4(a) was obtained with Eq. (5) and was used to obtain simulated profiles shown in Fig. 4(b). The numerical parameters employed in these simulations are also indicated in the figure. As a result, it was clearly indicated that the difference in HXPE and SXPE profile shown in Fig. 2 can be safely attributed to the difference in IMFP of photoelectrons. With these assumptions, ϕ_{b0} and N_D remain the only unknown

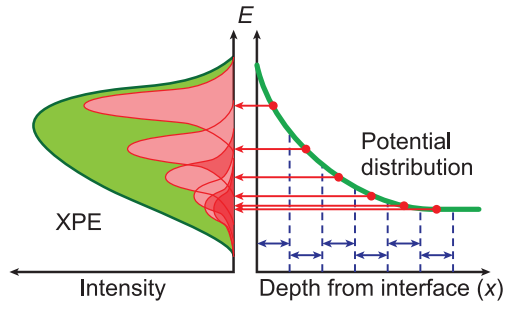

FIG. 3. Illustration of XPE profile simulation.

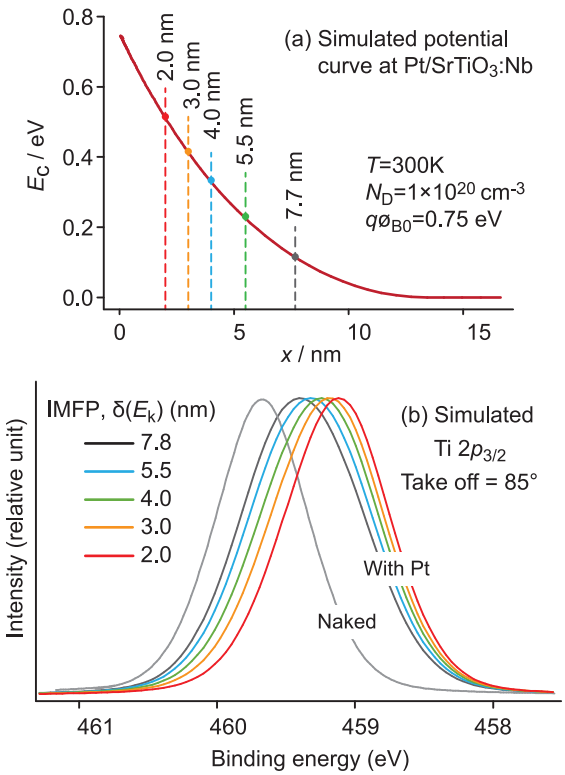

FIG. 4. Potential distribution ($E_c(x)$) at Pt/$SrTiO_3$:Nb junction (a) determined by entering parameters shown here into Eq. (5) and Ti 2 p XPE profile (b) simulated by entering $E_c(x)$ and various IMFPs into Eq. (4).

parameters for fitting simulated XPE profile to observed one. Thus, we performed simulations with various combinations of N_D and ϕ_{b0} to obtain the best fit between the observed and simulated XPE profiles. We note that while N_D, in principle, was determined in reference to the Hall measurements, it was used as a fitting parameter to obtain the best fit.

Figure 5 shows the optimized $E_c(x)$ resulting in the best fit between the simulated and observed HXPE spectra. The best fit was achieved when we assumed that $q\phi_{b0} = 0.75$ eV for both 0.05 and 0.5 wt. % Nb doped samples. Notably, the best fit of the observed SXPE profile to the model (not shown) was also achieved under this same assumption. Confirmation of the consistency between the simulations of SXPE and HXPE profiles indicates that the model we employed was reasonable. That is, the present results indicate that the assumption of the electric field dependence of ε_r (Eq. (1)) is reasonable for this system. Some other results of profile calculations are available to see elsewhere.[24]

As mentioned, the XPE profile, peak position, and width for the sample with high Nb concentration, i.e., 0.5 wt. %, slightly varied from sample to sample. In the context of the model employed here, this variation could be attributed to fluctuation of N_D at the surface. For the sample shown in Fig. 5(b), the N_D for the best fit was 1×10^{20} cm^{-3}, whereas the n determined by the Hall effect was 2×10^{20} cm^{-3}. Although such an inconsistency between the N_D determined by XPE fitting and the n determined by the Hall effect was seen in some samples, the best fit of the simulation was obtained by setting ϕ_{b0} to 0.7–0.8 V regardless of the Nb concentration and thickness of the Pt electrode. The variation of the peak position was attributed to change in non-stoichiometry and/or defect density due to polishing damage and/or annealing. Indeed, polishing is a potential cause for defect formation.[25]

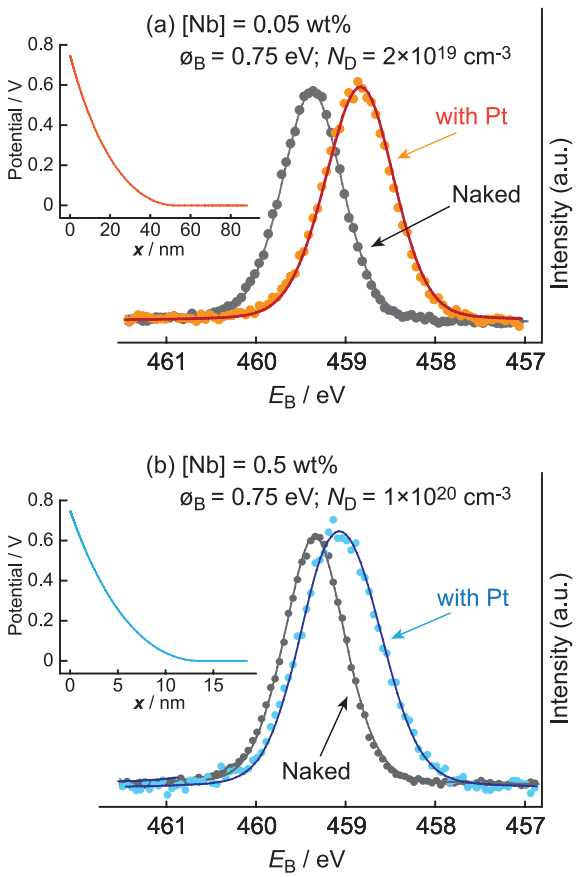

FIG. 5. Observed and simulated HXPE profiles. Solid lines and dots show simulated and observed XPE values, respectively. Inset shows potential profile in $SrTiO_3$:Nb determined by entering φ_B and N_D values shown here into Eq. (5).

The potential barrier at the Pt/$SrTiO_3$:Nb junction determined by the XPE method was 0.7–0.8 V in the present study, consistent with that reported in the literature.[15] This value is much lower than the barrier height determined by electric measurements. For instance, the barrier height was determined to be 1.1 V by current-voltage measurements.[15,26] The origin of this discrepancy is not identified in this study. One thing to be considered should be less pronounced hysteresis in I–V curve of the samples with thin Pt electrode used in this study (see Fig. 1). In our previous report,[9] it was indicated that RS behavior at Pt/$SrTiO_3$:Nb junction could be explained by assuming variation of $q\phi_{B0}$ along with RS behavior: $q\phi_{B0} = 1.2$ and 0.85 eV for high and low resistance state, respectively. The relatively high leakage current in the samples used in this study corresponds to the low resistance state of the samples considered in the previous report.[9] Looking at the potential profile ($E_c(x)$) to obtain the best fit between the observed and simulated XPE profile, the depletion layer width, W_d, was as narrow as 15 nm for the sample doped with 0.5 wt. % Nb doped sample and such very narrow W_d explains very high level of leakage current through tunneling process. Namely, we need to characterize samples under high resistance state to reveal the RS mechanism at Pt/$SrTiO_3$:Nb junctions.

In summary, we investigated the potential distribution at metal/$SrTiO_3$ junctions by XPE spectroscopy and obtained two major findings. First, the shift and broadening of the Ti 2p XPE peak of $SrTiO_3$:Nb beneath a Schottky Pt electrode were well reproduced with a model that assumed electric field dependence of ε in $SrTiO_3$:Nb. This leads us to conclude that quantitative analyses of the potential distribution in the Schottky junction are possible using XPE spectra. Second, the barrier height at the Pt/$SrTiO_3$:Nb junction was determined to be 0.7–0.8 V, which was much less than that estimated from electric and optical measurements. This is crucial knowledge toward a complete understanding of the RS behavior at metal/$SrTiO_3$ junctions. The reason for the discrepancy between the electric measurements and XPE results must be identified to clarify the nature of metal/$SrTiO_3$:Nb junctions.

Part of this study was supported by a Grant-in-Aid for the World Premier Research Institute Initiative promoted by the Ministry of Education, Culture, Sports, Science, and Technology (MEXT), Japan. This study was also partially supported by Kaken-hi from the Japan Society for Promotion of Science (JSPS) and MEXT, Japan. The HXPES measurements were performed under the approval of the NIMS Beamline Station. The authors are grateful to HiSOR, Hiroshima Univ., and JAEA/SPring-8 for the development of the HXPES instrumentation at BL15XU, SPring-8. The extensive efforts by Mr. Tomohiro Furuta and Mr. Hiroki Miyazaki of Hosei University, Tokyo, on HXPES measurements are also acknowledged.

[1]J. Fleig, S. Rodewald, and J. Maier, J. Appl. Phys. **87**, 2372 (2000).
[2]K. Hayashi, T. Yamamoto, Y. Ikuhara, and T. Sakuma, J. Appl. Phys. **86**, 2909 (1999).
[3]T. Shimizu and H. Okushi, J. Appl. Phys. **85**, 7244 (1999).
[4]C. Park, Y. Seo, J. Jung, and D. W. Kim, J. Appl. Phys. **103**, 054106 (2008).
[5]D. S. Shang, J. R. Sun, L. Shi, and B. G. Shen, Appl. Phys. Lett. **93**, 102106 (2008).
[6]Y. Watanabe, Appl. Phys. Lett. **66**, 28 (1995).
[7]A. Beck, J. G. Bednorz, C. Gerber, C. Rossel, and D. Widmer, Appl. Phys. Lett. **77**, 139 (2000).
[8]T. Fujii, M. Kawasaki, A. Sawa, Y. Kawazoe, H. Akoh, and Y. Tokura, Phys. Rev. B **75**, 165101 (2007).
[9]J. Li, N. Ohashi, H. Okushi, and H. Haneda, Phys. Rev. B **83**, 125317 (2011), and references therein.
[10]S. M. Sze, *Physics of Semiconductor Devices*, 2nd ed. (John Wiley & Sons, New York, 1981).
[11]T. Yamamoto, S. Suzuki, H. Suzuki, K. Kawaguchi, and K. Takahashi, Jpn. J. Appl. Phys. **37**, 4737 (1998), and references therein.
[12]T. Susaki, Y. Kozuka, Y. Tateyama, and H. Y. Hwang, Phys. Rev. B **76**, 155110 (2007), and references therein.
[13]E. Sawaguchi, A. Kikuchi, and Y. Kodera, J. Phys. Soc. Jpn. **17**, 1666 (1962).
[14]J. H. Barrett, Phys. Rev. **86**, 118 (1952).
[15]R. Schafranek, S. Payan, M. Maglione, and A. Klein, Phys. Rev. B **77**, 195310 (2008).
[16]M. Copel, P. R. Duncombe, D. A. Neumayer, T. M. Shaw, and R. M. Trompn, Appl. Phys. Lett. **70**, 3227 (1997).
[17]R. Schafranek and A. Klein, Solid State Ionics **177**, 1659 (2006).
[18]S. Ueda, Y. Katsuya, M. Tanaka, H. Yoshikawa, Y. Yamashita, S. Ishimaru, Y. Matsushita, and K. Kobayashi, AIP Conf. Proc. **1234**, 403 (2010).
[19]K. Kobayashi, Nucl. Instrum. Methods Phys. Res. A **601**, 32 (2009).
[20]T. Nagata, O. Bierwagen, M. E. White, M. Y. Tsai, Y. Yamashita, H. Yoshikawa, N. Ohashi, K. Kobayashi, T. Chikyow, and J. S. Speck, Appl. Phys. Lett. **98**, 232107 (2011).
[21]B. Li, Y. Adachi, J. Li, H. Okushi, I. Sakaguchi, S. Ueda, H. Yoshikawa, Y. Yamashita, S. Senju, K. Kobayashi, M. Sumiya, H. Haneda, and N. Ohashi, Appl. Phys. Lett. **98**, 082101 (2011).
[22]J. R. Williams, I. Píš, M. Kobata, A. Winkelmann, T. Matsushita, Y. Adachi, N. Ohashi, and K. Kobayashi, J. Appl. Phys. **111**, 033525 (2012).
[23]S. Tanuma, C. J. Powell, and D. R. Penn, Surf. Interface Anal. **21**, 165 (1994).
[24]See supplementary material at http://dx.doi.org/10.1063/1.4772628 for SXPES profile fitting and additional information.
[25]H. Miyazaki, Y. Adachi, I. Sakaguchi, T. Ishigaki, and N. Ohashi, Key Eng. Mater. **485**, 215 (2011).
[26]G. W. Dietz, W. Antpöhler, M. Klee, and R. Waser, J. Appl. Phys. **78**, 6113 (1995).